Influence of the finite element type of the sleeper on vehicle-track interaction: a numerical study

Xu, Lei; Lu, Tao

DOI
10.1080/00423114.2020.1769847

Publication date
2020

Document Version
Final published version

Published in
Vehicle System Dynamics: international journal of vehicle mechanics and mobility

Taylor & Francis
Taylor & Francis Group

Vehicle System Dynamics
International Journal of Vehicle Mechanics and Mobility

ISSN: (Print) (Online) Journal homepage: https://www.tandfonline.com/loi/nvsd20

Influence of the finite element type of the sleeper on vehicle-track interaction: a numerical study

Lei Xu & Tao Lu

To cite this article: Lei Xu & Tao Lu (2021) Influence of the finite element type of the sleeper on vehicle-track interaction: a numerical study, Vehicle System Dynamics, 59:10, 1533-1556, DOI: 10.1080/00423114.2020.1769847

To link to this article: https://doi.org/10.1080/00423114.2020.1769847

Published online: 24 May 2020.

VEHICLE SYSTEM DYNAMICS
2021, VOL. 59, NO. 10, 1533–1556
https://doi.org/10.1080/00423114.2020.1769847

Influence of the finite element type of the sleeper on vehicle-track interaction: a numerical study

Lei Xu[a] and Tao Lu [b]

[a]School of Civil Engineering, Central South University, Changsha, People's Republic of China; [b]Delft University of Technology, Faculty of Civil Engineering and Geosciences, Railway Engineering Group, Delft, the Netherlands

ABSTRACT

In the framework of vehicle-track interaction, this work puts an emphasis on clarifying the influence of sleeper finite element types on system dynamic responses. Three sleeper element types, namely the rigid-body, extensible Euler-Bernoulli beam and solid element are used respectively in the track system modelling with detail mathematical formulations presented. The rails are modelled as Timoshenko beams. The ballasted track system is subject to a moving vehicle with coupled wheel-rail interactions. From aspects of both frequency- and time- domain analysis in the numerical study, the effectiveness of this model has been validated. The influences of the sleeper finite element type, the sleeper support stiffness and damping coefficient on the system responses have been investigated.

ARTICLE HISTORY
Received 17 February 2020
Revised 8 April 2020
Accepted 9 May 2020

KEYWORDS
Vehicle-track interaction; sleeper finite element; frequency response function

1. Introduction

In commonly built tracks and heavy haul lines, ballasted tracks are widely used, where the railway sleepers play a vital role in supporting the rails, spreading the pressure from the moving trains to the ballast layer and holding the rail gauge width and inclination, etc. It has therefor long been conscious of the importance to study the influence of sleeper vibration characteristics on railway engineering evaluation and management. See for instance, the performance improvement [1,2], damage detection [3–5] and dynamic analysis [6,7] of sleepers have attracted more and more attention from railway researchers and engineers.

Unlike in situ or laboratory experimental studies [3,8–11] which require large financial arrangements, modelling of railway tracks has been a hot topic accompanied by the development of computer technologies since it is economical and efficient. Early in 1995, in the work of Grassie [12], the length, the mass and the cross-sectional dimensions for totally 12 sleepers of different types were tested and summarized, and then experiments were conducted to calculate natural frequencies of the sleepers. A simple dynamic model for monobloc concrete sleepers with non-uniform cross-sections had been derived using Timoshenko beam theory. To consider both rails in railway tracks supported by

CONTACT Tao Lu T.Lu-2@tudelft.nl

continuous foundation, Tran et al. [13] presented an analytical model including two rails supported by sleepers, where the sleepers were modelled as Euler-Bernoulli beams by introducing the Green's function and the relation between the rail reaction force and the rail displacement in frequency domain. Using finite element package such as ANSYS®, Kaewunruen and Remennikov [14] employed the solid element SOLID65 and nonlinear material constitutive to characterise the tension cracking and the compression crushing of sleepers.

The above researches facilitate the understanding of sleepers on their mechanical behaviours and frequency characteristics. However, the coupled interaction between the running vehicle and the tracks is neglected by only loading the moving loads unidirectionally. Regarding this matter, many scholars have conducted extensive researches considering the cooperation of vehicular excitations and its interaction. Sadri et al. [15] presented a frequency domain model with a double periodicity layer where the sleeper periodicity and the non-uniformity of track properties can be considered, besides the vehicle is assumed as a moving mass wheel; Aiming at investigating the dynamic behaviour of a typical prestressed concrete sleeper, Kumaran et al. [16] developed a time domain model using MSC/NASTRAN software considering wheel-track dynamic interaction, moreover, the effects of wheel/rail imperfections and various parametric conditions are discussed. In their work, solid finite elements are implemented to model the rail, the sleeper and the sub-ballast, thus limited to 12 sleepers due to high degrees of freedom (d.o.f.). In the work of Zhai et al. [17], refinement of wheel-rail contacts at 3-D space is put on the emphasis for constructing the vehicle-track coupled model. In the ballasted tracks, the sleepers are modelled as mass elements with the vertical-, the lateral- and the rolling- motion considered. Similar work had also been carried out in [18–21].

Highlighting vehicle-track interaction in a coupled way, considerable researches have been done but a dedicated work investigating the influence of sleeper model on system performance is rather rare and has not given special attention. With a summation, the rigid-body sleeper [17,18], elastic-beam sleeper [12] and solid sleeper [14] have been adopted in vehicle-track modelling construction, but the analysis on clarifying the applicability and engineering practicality of the sleeper model is not revealed.

The aim of this work is therefore to take an investigation into the effects of sleeper modelling differences on vehicle-track interaction. Vehicle-track interaction model will be firstly established in Section 2 considering moving vehicles on tracks modelled by finite element method. Then the mathematical formulation for constructing ballasted tracks by different finite elemental types will be presented in Section 3. To investigate the vibration characteristics of system components in frequency- and time- domain, its precondition is solving the dynamics equation of motion for vehicle-track interaction, as shown in Section 4. Numerical examples will be presented in Section 5 to validate this model and to show the dynamic influence of sleeper finite element types on system vibrations and finally concluding remarks will be derived this work.

2. Dynamic model for vehicle-ballast track interaction

In this work, a three-dimensional vehicle-ballast track interaction model, as shown in Figure 1, is developed based on the vehicle-track coupled dynamics theory [22]. Without loss of generality, the dynamic equations of motion for vehicle-ballast track interaction

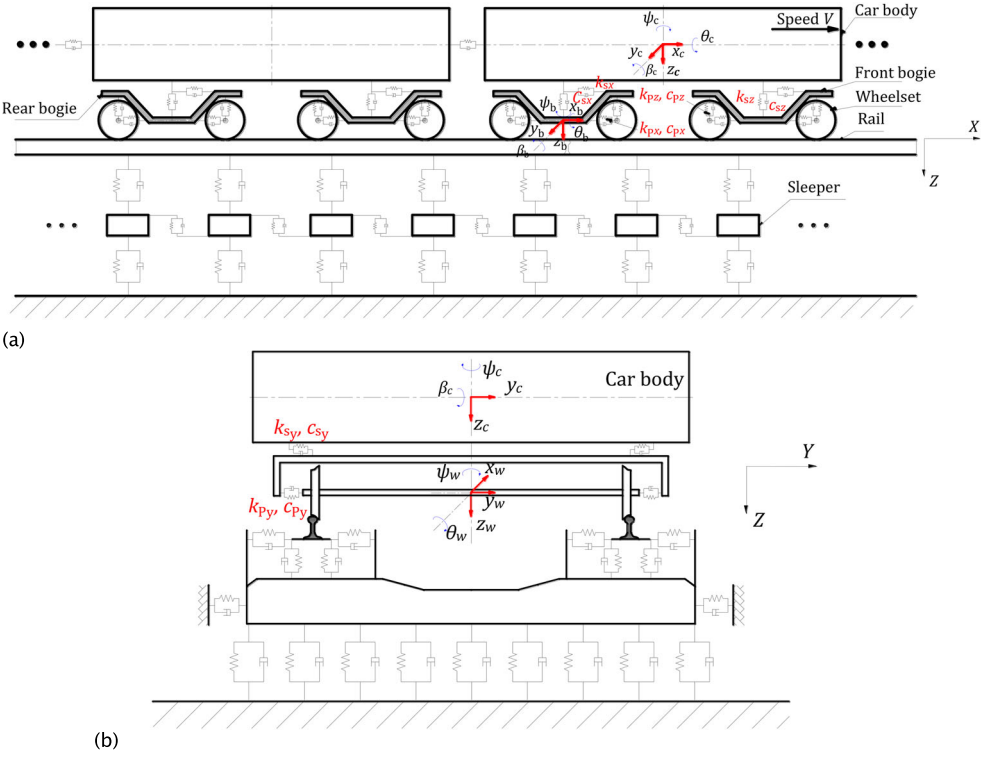

Figure 1. Vehicle-ballast track interaction model (a. side view; b. end view).

can be expressed by

$$\begin{bmatrix} \mathbf{M}_{VV} & \mathbf{0} \\ \mathbf{0} & \mathbf{M}_{TT} \end{bmatrix} \begin{Bmatrix} \ddot{\mathbf{X}}_V \\ \ddot{\mathbf{X}}_T \end{Bmatrix} + \begin{bmatrix} \mathbf{C}_{VV} & \mathbf{0} \\ \mathbf{0} & \mathbf{C}_{TT} \end{bmatrix} \begin{Bmatrix} \dot{\mathbf{X}}_V \\ \dot{\mathbf{X}}_T \end{Bmatrix} + \begin{bmatrix} \mathbf{K}_{VV} & \mathbf{0} \\ \mathbf{0} & \mathbf{K}_{TT} \end{bmatrix} \begin{Bmatrix} \mathbf{X}_V \\ \mathbf{X}_T \end{Bmatrix} = \begin{bmatrix} \mathbf{F}_V \\ \mathbf{F}_T \end{bmatrix} \tag{1}$$

where $\mathbf{M}$, $\mathbf{C}$ and $\mathbf{K}$ denote the mass, damping and stiffness matrices respectively; the subscripts 'V' and 'T' indicate quantities for the systems of the vehicle and the track, respectively; $\ddot{\mathbf{X}}$, $\dot{\mathbf{X}}$ and $\mathbf{X}$ denote the acceleration, velocity and displacement vectors, respectively; $\mathbf{F}$ denotes the loading vector.

The vehicle is modelled as a multi-rigid-body system including one car body, two bogie frames and four wheelsets, and each body possesses six degrees of freedom (d.o.f.), i.e. the linear displacements (x, y and z) along the X-, Y- and Z- axes and yaw, pitch and rolling angle (ψ, β and θ) around Z-, Y- and X-axis respectively. The car body is connected to the bogie frames by the secondary suspension system, and the bogie frames and the wheelsets are connected by the primary suspension system.

The ballast track system consists of the rail modelled by Timoshenko beams and the sleepers modelled by the rigid body, the elastic beam such as Bernoulli-Euler beam and the solid element. The rail pads are modelled as spring-dashpot elements connecting the rail and the sleeper. The interaction between sleepers induced by the friction of ballast particles

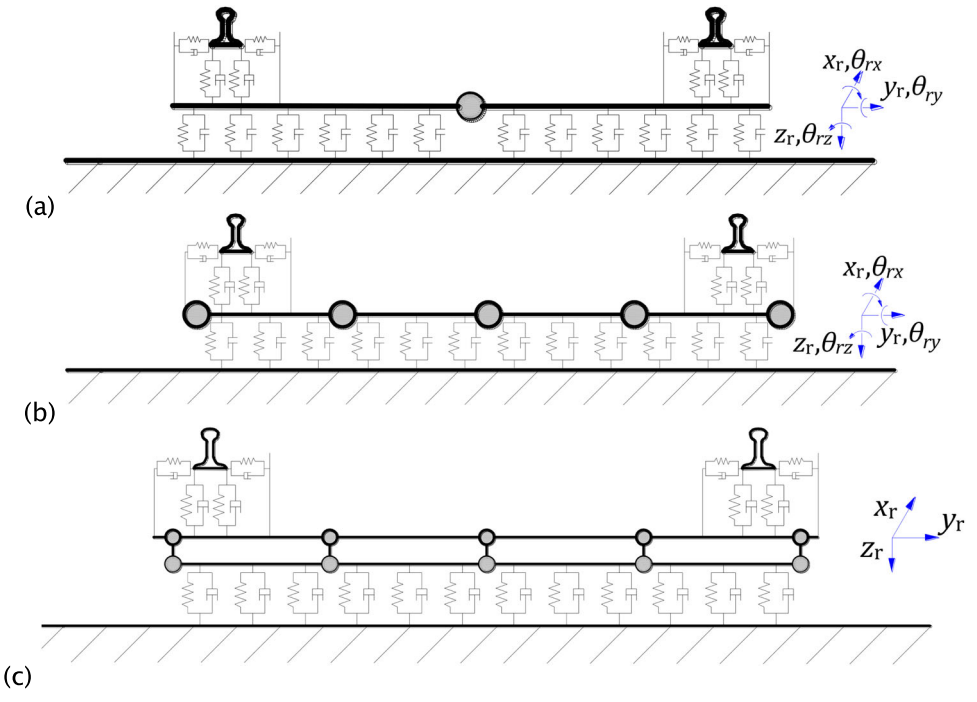

Figure 2. Ballast track model for different finite elemental sleepers, end view. (a. rigid body sleeper; b. elastic-beam element sleeper; c. solid element sleeper).

is also equivalently depicted by spring-dashpot elements. The bottom of the sleepers is continuous supported by linear springs and dashpots.

To couple the vehicle and the track in light of the wheel-rail interfacial contact, a wheel-rail spatially coupling model in [17] is compiled into this vehicle-track interaction programme.

3. Modelling of sleepers using various finite elements

In the next Subsections, the modelling matrices for the rigid-body element, the elastic-beam element and the solid element sleepers, as shown in Figure 2, will be respectively illustrated.

3.1. Rigid-body element sleeper

If the sleeper is modelled as a rigid body element, the work done by the inertial effects caused by the mass is considered, and accordingly the mass matrices of the sleeper can be harvested by

$$\mathbf{M}_{ss} = \sum_i \mathbf{M}_{ss,i} \tag{2}$$

with $\mathbf{M}_{ss,i} = \text{diag}\left(\begin{bmatrix} m_s & m_s & m_s & J_{s,x} & J_{s,y} & J_{s,z} \end{bmatrix}\right)$,

where the subscript 'i' denotes the ith sleeper; m_s is the sleeper mass, and $J_{s,x}$, $J_{s,y}$ and $J_{s,z}$ denote respectively the moment of inertia around X-, Y- and Z-axis at the sleeper centroid.

3.1.1. Interaction matrices between the rail and the sleeper

The rail-sleeper interaction stiffness and damping matrices can be derived by the elastic deformational energy of the rail pads and the negative value of the work done by the damping force between the rail and the sleeper respectively, that is,

$$\begin{cases} \mathbf{K}_{\mathrm{rs}} = \sum_i \sum_j (\mathbf{K}_{\mathrm{rs},X,i,j} + \mathbf{K}_{\mathrm{rs},Y,i,j} + \mathbf{K}_{\mathrm{rs},Z,i,j}) \\ \mathbf{C}_{\mathrm{rs}} = \sum_i \sum_j (\mathbf{C}_{\mathrm{rs},X,i,j} + \mathbf{C}_{\mathrm{rs},Y,i,j} + \mathbf{C}_{\mathrm{rs},Z,i,j}) \end{cases} \tag{3}$$

with

$$\begin{aligned}
\mathbf{K}_{\mathrm{rs},X,i,j} &= k_{\mathrm{rs},x}([\mathbf{N}^x_{\mathrm{r},j}] - [\mathbf{N}^x_{\mathrm{s},j}])^{\mathrm{T}}([\mathbf{N}^x_{\mathrm{r},j}] - [\mathbf{N}^x_{\mathrm{s},j}]), \\
[\mathbf{N}^x_{\mathrm{r},j}] &= [\,\cdots\ 0\ \cdots\ 1{-}\xi_{\mathrm{r},j}\ \xi_{\mathrm{r},j}\ \cdots\ 0\ \cdots\,], \quad \xi_{\mathrm{r},j} = x_{\mathrm{r},j}/l_{\mathrm{r}}, \\
[\mathbf{N}^x_{\mathrm{s},j}] &= [\,\cdots\ 0\ \cdots\ 1\ (-1)^{j+1}y_{\mathrm{s},j}\ -l_H/2\ \cdots\ 0\ \cdots\,], \quad y_{\mathrm{s},j} = w_{\mathrm{s}}/2 - b, \\
\mathbf{K}_{\mathrm{rs},Y,i,j} &= k_{\mathrm{rs},y}([\mathbf{N}^y_{\mathrm{r},j}] - [\mathbf{N}^y_{\mathrm{s},j}])^{\mathrm{T}}([\mathbf{N}^y_{\mathrm{r},j}] - [\mathbf{N}^y_{\mathrm{s},j}]), \\
[\mathbf{N}^y_{\mathrm{r},j}] &= [\cdots\ 0\ \cdots\ 1 - 3\xi^2_{\mathrm{r},j} + 2\xi^3_{\mathrm{r},j}\ \ (\xi_{\mathrm{r},j} - 2\xi^2_{\mathrm{r},j} - \xi^3_{\mathrm{r},j})l_{\mathrm{r}}\ \ 3\xi^2_{\mathrm{r},j} \\
&\quad - 2\xi^3_{\mathrm{r},j}\ \ (\xi^3_{\mathrm{r},j} - \xi^2_{\mathrm{r},j})l_{\mathrm{r}}\ \ \cdots\ \ 0\ \ \cdots], \\
[\mathbf{N}^y_{\mathrm{s},j}] &= [\,\cdots\ 0\ \cdots\ 1\ l_H/2\ x_{\mathrm{s},j}\ \cdots\ 0\ \cdots\,], \mathbf{K}_{\mathrm{rs},Z,i,j} = k_{\mathrm{rs},z}([\mathbf{N}^z_{\mathrm{r},j}] - [\mathbf{N}^z_{\mathrm{s},j}])^{\mathrm{T}}([\mathbf{N}^z_{\mathrm{r},j}] - [\mathbf{N}^z_{\mathrm{s},j}]), \\
[\mathbf{N}^z_{\mathrm{r},j}] &= [\cdots\ 0\ \cdots\ 1 - 3\xi^2_{\mathrm{r},j} + 2\xi^3_{\mathrm{r},j}\ \ -(\xi_{\mathrm{r},j} - 2\xi^2_{\mathrm{r},j} - \xi^3_{\mathrm{r},j})l_{\mathrm{r}}\ \ 3\xi^2_{\mathrm{r},j} \\
&\quad - 2\xi^3_{\mathrm{r},j}\ \ -(\xi^3_{\mathrm{r},j} - \xi^2_{\mathrm{r},j})l_{\mathrm{r}}\ \ \cdots\ \ 0\ \ \cdots] \\
[\mathbf{N}^z_{\mathrm{s},j}] &= [\cdots\ 0\ \cdots\ 1\ \ (-1)^j y_{\mathrm{s},j}\ \ -x_{\mathrm{s},j}\ \ \cdots\ \ 0\ \ \cdots,
\end{aligned}$$

where the subscript 'j' indicates the location of the rail seat; $\mathbf{K}_{\mathrm{rs},X,i,j}$, $\mathbf{K}_{\mathrm{rs},Y,i,j}$ and $\mathbf{K}_{\mathrm{rs},Z,i,j}$ denote respectively the rail-sleeper longitudinal, lateral and vertical interaction stiffness matrix; $k_{\mathrm{rs},x}$, $k_{\mathrm{rs},y}$ and $k_{\mathrm{rs},z}$ denote the rail-sleeper longitudinal, lateral and vertical interaction stiffness coefficient; l_{r} is the length of a rail element and w_{s} is the width of the sleeper; b is the distance between the left-side of the sleeper and the rail-sleeper contact point along the Y-axis direction; l_H is the height of the sleeper and $x_{\mathrm{s},j}$ is the distance between the rail-sleeper contact point and the sleeper centroid along the X-axis direction; the damping matrices $\mathbf{C}_{\mathrm{rs},X,i,j}$, $\mathbf{C}_{\mathrm{rs},Y,i,j}$ and $\mathbf{C}_{\mathrm{rs},Z,i,j}$ have respectively the same expressions as $\mathbf{K}_{\mathrm{rs},X,i,j}$, $\mathbf{K}_{\mathrm{rs},Y,i,j}$ and $\mathbf{K}_{\mathrm{rs},Z,i,j}$, only needing to substitute the stiffness coefficients $k_{\mathrm{rs},x}$, $k_{\mathrm{rs},y}$ and $k_{\mathrm{rs},z}$ with damping coefficients $c_{\mathrm{rs},x}$, $c_{\mathrm{rs},y}$ and $c_{\mathrm{rs},z}$.

It should be noted that the non-zero quantities of the shape function $[\mathbf{N}]$ are actually corresponding to specific degrees of freedom of the finite elements. The basic methodology and principle for deriving above equations have been presented in [18] with details, which can be referred to.

3.1.2. Interaction matrices between the sleeper and the subgrade

The role of the railway ballast is offering the elastic supports and absorbing the vibration energy, which is regarded as continuous support stiffness and damping coefficients underneath the sleeper. The interaction stiffness and damping matrices, denoted by $\mathbf{K}_{\mathrm{ss}'}$ and $\mathbf{C}_{\mathrm{ss}'}$

respectively, between the sleeper and the constraint subgrade can be harvested by

$$\begin{cases} \mathbf{K}_{ss'} = \sum_i (\mathbf{K}_{ss',X,i} + \mathbf{K}_{ss',Y,i} + \mathbf{K}_{ss',Z,i}) \\ \mathbf{C}_{ss'} = \sum_i (\mathbf{C}_{ss',X,i} + \mathbf{C}_{ss',Y,i} + \mathbf{C}_{ss',Z,i}) \end{cases} \tag{4}$$

with

$$\begin{aligned} \mathbf{K}_{ss',X,i} &= k_{ss',x} \int_{-w_s/2}^{w_s/2} \int_{-l_W/2}^{l_W/2} [\mathrm{N}_{ss',x}]^{\mathrm{T}} [\mathrm{N}_{ss',x}] \mathrm{d}y_s \mathrm{d}z_s, \\ \mathrm{N}_{ss',x}] &= [\cdots \quad 0 \quad \cdots \quad 1 \quad -y_s \quad z_s \quad \cdots \quad 0 \quad \cdots], \\ \mathbf{K}_{ss',Y,i} &= k_{ss',y} w_s \int_{-l_H/2}^{l_H/2} [\mathrm{N}_{ss',y}]^{\mathrm{T}} [\mathrm{N}_{ss',y}] \mathrm{d}z_s, \\ \mathrm{N}_{ss',y}] &= [\cdots \quad 0 \quad \cdots \quad 1 \quad \frac{l_W}{2} \quad -z_s \quad \cdots \quad 0 \quad \cdots], \\ \mathbf{K}_{ss',Z,i} &= k_{ss',z} \int_{-w_s/2}^{w_s/2} \int_{-l_W/2}^{l_W/2} [\mathrm{N}_{ss',z}]^{\mathrm{T}} [\mathrm{N}_{ss',z}] \mathrm{d}x_s \mathrm{d}y_s, \\ [\mathrm{N}_{ss',z}] &= \left[\cdots \quad 0 \quad \cdots \quad 1 \quad -x_s \quad y_s \quad \cdots \quad 0 \quad \cdots \right], \end{aligned}$$

where $k_{ss',x}$, $k_{ss',y}$ and $k_{ss',z}$ denote respectively equivalent longitudinal, lateral and vertical stiffness coefficients provided by the railway ballast; l_W is the width of the sleeper at the end cross-section; the damping matrices $\mathbf{C}_{ss',X,i}$, $\mathbf{C}_{ss',Y,i}$ and $\mathbf{C}_{ss',Z,i}$ have the same expressions as $\mathbf{K}_{ss',X,i}$, $\mathbf{K}_{ss',Y,i}$ and $\mathbf{K}_{ss',Z,i}$ just needing to substitute the stiffness coefficients '$k_{ss',x}$', '$k_{ss',y}$' and '$k_{ss',z}$' with the damping coefficients '$c_{ss',x}$', '$c_{ss',y}$' and '$c_{ss',z}$'.

3.2. Elastic-beam element sleeper

In this section, the sleeper is modelled as an extensible Euler-Bernoulli beam. Once the sleeper is modelled as an elastic-beam element, the work done by the inertial forces and the elastically axial- and bending- strain energy of the sleeper should be accounted for, and the mass and stiffness matrices of the sleeper can be represented by $\mathbf{M}_{ss}$ and $\mathbf{K}_{ss}$. The method for deriving $\mathbf{M}_{ss}$ and $\mathbf{K}_{ss}$ is omitted here for brevity and can be referred to [19].

3.2.1. Interaction matrices between the rail and the sleeper

The rail-sleeper interaction stiffness and damping matrices can be derived by the elastic deformational energy of the rail pads and the negative value of the work done by the damping force between the rail and the sleeper respectively, that is,

$$\begin{cases} \mathbf{K}_{rs} = \sum_i \sum_j (\mathbf{K}_{rs,X,i,j} + \mathbf{K}_{rs,Y,i,j} + \mathbf{K}_{rs,Z,i,j}) \\ \mathbf{C}_{rs} = \sum_i \sum_j (\mathbf{C}_{rs,X,i,j} + \mathbf{C}_{rs,Y,i,j} + \mathbf{C}_{rs,Z,i,j}) \end{cases} \tag{5}$$

with

$$\mathbf{K}_{\mathrm{rs},X,i,j} = k_{\mathrm{rs},x}\left([\mathbf{N}^x_{\mathrm{r},j}] - [\mathbf{N}^x_{\mathrm{s},j}] + \frac{l_H}{2}[\mathbf{N}^{\theta_Y}_{\mathrm{s},j}]\right)^{\mathrm{T}}\left([\mathbf{N}^x_{\mathrm{r},j}] - [\mathbf{N}^x_{\mathrm{s},j}] + \frac{l_H}{2}[\mathbf{N}^{\theta_Y}_{\mathrm{s},j}]\right)$$

$$\mathbf{N}^x_{\mathrm{s},j}] = \left[\cdots\ 0\ \cdots\ 1{-}3\xi^2_{\mathrm{s},j}{+}2\xi^3_{\mathrm{s},j}\ -(\xi_{\mathrm{s},j}{-}2\xi^2_{\mathrm{s},j}{-}\xi^3_{\mathrm{s},j})w_{\mathrm{s}}\ 3\xi^2_{\mathrm{s},j}{-}2\xi^3_{\mathrm{s},j}\ -(\xi^3_{\mathrm{s},j}{-}\xi^2_{\mathrm{s},j})w_{\mathrm{s}}\ \cdots\ 0\ \cdots\right]\ \xi_{\mathrm{s},j} = y_{\mathrm{s},j}/w_{\mathrm{s}}$$

$$y_{\mathrm{s},j} = \begin{cases} b - (n_j - 1)w_{\mathrm{s}} \text{ when } j = 1 \\ (W_{\mathrm{s}} - b) - (n_j - 1)w_{\mathrm{s}} \text{ when } j = 2 \end{cases}$$

$$n_j = \begin{cases} \Upsilon(b/w_{\mathrm{s}}) + 1 \text{ when } j = 1 \\ \Upsilon((W_{\mathrm{s}} - b)/w_{\mathrm{s}}) + 1 \text{ when } j = 2 \end{cases}$$

$$[\mathbf{N}^{\theta_Y}_{\mathrm{s},j}] = \left[\ \cdots\quad 0\quad \cdots\quad 1 - \xi_{\mathrm{s},j}\quad \xi_{\mathrm{s},j}\quad \cdots\quad 0\quad \cdots\ \right]$$

$$\mathbf{K}_{\mathrm{rs},Y,i,j} = k_{\mathrm{rs},y}([\mathbf{N}^y_{\mathrm{r},j}] - [\mathbf{N}^y_{\mathrm{s},j}])^{\mathrm{T}}([\mathbf{N}^y_{\mathrm{r},j}] - [\mathbf{N}^y_{\mathrm{s},j}]) \quad [\mathbf{N}^y_{\mathrm{s},j}] = [\mathbf{N}^{\theta_Y}_{\mathrm{s},j}]$$

$$\mathbf{K}_{\mathrm{rs},Z,i,j} = k_{\mathrm{rs},z}([\mathbf{N}^z_{\mathrm{r},j}] - [\mathbf{N}^z_{\mathrm{s},j}])^{\mathrm{T}}([\mathbf{N}^z_{\mathrm{r},j}] - [\mathbf{N}^z_{\mathrm{s},j}]), \mathbf{N}^z_{\mathrm{s},j}] = [\mathbf{N}^x_{\mathrm{s},j}]$$

where $j = 1{,}2$ denote respectively the left- and right- side of the rail seat for a sleeper; W_{s} is the total length of a sleeper; $\Upsilon(\cdot)$ is an operator rounding each element towards the nearest integer.

3.2.2. Interaction matrices between the sleeper and the subgrade

The interaction stiffness and damping matrices, denoted by $\mathbf{K}_{\mathrm{ss}'}$ and $\mathbf{C}_{\mathrm{ss}'}$ respectively, between the sleeper and the constraint subgrade can be harvested by

$$\begin{cases} \mathbf{K}_{\mathrm{ss}'} = \sum_i \sum_k (\mathbf{K}_{\mathrm{ss}',X,i} + \mathbf{K}_{\mathrm{ss}',Y,i} + \mathbf{K}_{\mathrm{ss}',Z,i}) \\ \mathbf{C}_{\mathrm{ss}'} = \sum_i \sum_k (\mathbf{C}_{\mathrm{ss}',X,i} + \mathbf{C}_{\mathrm{ss}',Y,i} + \mathbf{C}_{\mathrm{ss}',Z,i}) \end{cases} \tag{6}$$

with

$$\mathbf{K}_{\mathrm{ss}',X,i} = k_{\mathrm{ss}',x} l_H \int_0^{w_{\mathrm{s}}} [\mathbf{N}_{\mathrm{ss}',x}]^{\mathrm{T}}[\mathbf{N}_{\mathrm{ss}',x}]\mathrm{d}y_{\mathrm{s}}, \quad [\mathbf{N}_{\mathrm{ss}',x}] = [\mathbf{N}^x_{\mathrm{s},j}]$$

$$\mathbf{K}_{\mathrm{ss}',Y,i} = k_{\mathrm{ss}',y} l_H \int_0^{w_{\mathrm{s}}} [\mathbf{N}_{\mathrm{ss}',y}]^{\mathrm{T}}[\mathbf{N}_{\mathrm{ss}',y}]\mathrm{d}y_{\mathrm{s}},$$

$$\mathbf{N}_{\mathrm{ss}',x}] = \left[\ \cdots\quad 0\quad \cdots\quad 1 - \xi_{\mathrm{s},k}\quad \xi_{\mathrm{s},k}\quad \cdots\quad 0\quad \cdots\ \right], \quad \xi_{\mathrm{s},k} = y_{\mathrm{s}}/w_{\mathrm{s}};$$

$$\mathbf{K}_{\mathrm{ss}',Z,i} = k_{\mathrm{ss}',z} l_W \int_0^{w_{\mathrm{s}}} [\mathbf{N}_{\mathrm{ss}',z}]^{\mathrm{T}}[\mathbf{N}_{\mathrm{ss}',z}]\mathrm{d}y_{\mathrm{s}}, \quad [\mathbf{N}_{\mathrm{ss}',z}] = [\mathbf{N}^x_{\mathrm{s},j}].$$

where the damping matrices $\mathbf{C}_{\mathrm{ss}',X,i}$, $\mathbf{C}_{\mathrm{ss}',Y,i}$ and $\mathbf{C}_{\mathrm{ss}',Z,i}$ have the same expressions as $\mathbf{K}_{\mathrm{ss}',X,i}$, $\mathbf{K}_{\mathrm{ss}',Y,i}$ and $\mathbf{K}_{\mathrm{ss}',Z,i}$ just needing to substitute the stiffness coefficients '$k_{\mathrm{ss}',x}$', '$k_{\mathrm{ss}',y}$' and '$k_{\mathrm{ss}',z}$' with the damping coefficients '$c_{\mathrm{ss}',x}$', '$c_{\mathrm{ss}',y}$' and '$c_{\mathrm{ss}',z}$'.

3.3. 8-node solid element sleeper

Once the sleeper is modelled as the combination of 8-node solid elements, the method for deriving $\mathbf{M}_{ss}$ and $\mathbf{K}_{ss}$ can be referred to [19] as similar to the modelling of the subgrade system, here not presented for brevity

3.3.1. Interaction matrices between the rail and the sleeper

Being similar to Equations (3) and (5), the rail-sleeper interaction stiffness and damping matrices can be also obtained by

$$\begin{cases} \mathbf{K}_{rs} = \sum_i \sum_j (\mathbf{K}_{rs,X,i,j} + \mathbf{K}_{rs,Y,i,j} + \mathbf{K}_{rs,Z,i,j}) \\ \mathbf{C}_{rs} = \sum_i \sum_j (\mathbf{C}_{rs,X,i,j} + \mathbf{C}_{rs,Y,i,j} + \mathbf{C}_{rs,Z,i,j}) \end{cases} \tag{7}$$

with

$$\begin{aligned}
\mathbf{K}_{rs,X,i,j} &= k_{rs,x}([\mathbf{N}^x_{r,j}] - [\mathbf{N}^x_{s,j}])^{\mathrm{T}}([\mathbf{N}^x_{r,j}] - [\mathbf{N}^x_{s,j}]),\\
[\mathbf{N}^x_{s,j}] &= [\cdots \quad N_1 \quad 0 \quad 0 \quad N_2 \quad 0 \quad 0 \quad N_3 \quad 0 \quad 0 \quad N_4 \quad 0 \quad 0 \quad N_5 \quad 0 \quad 0 \quad N_6\\
&\qquad 0 \quad 0 \quad N_7 \quad 0 \quad 0 \quad N_8 \quad 0 \quad 0 \quad \cdots]\\
N_1 &= (1-s)(1-t)(1-g)/8, \quad N_2 = (1-s)(1+t)(1-g)/8,\\
N_3 &= (1-s)(1-t)(1+g)/8, \quad N_4 = (1-s)(1+t)(1+g)/8,\\
N_5 &= (1+s)(1-t)(1-g)/8 \quad N_6 = (1+s)(1+t)(1-g)/8,\\
N_7 &= (1+s)(1-t)(1+g)/8, \quad N_8 = (1+s)(1+t)(1+g)/8,\\
s &= 0, \quad t = (y_{s,j} - (n_j - 1)w_s - w_s/2)/(w_s/2), \quad g = -1;\\
\mathbf{K}_{rs,Y,i,j} &= k_{rs,y}([\mathbf{N}^y_{r,j}] - [\mathbf{N}^y_{s,j}])^{\mathrm{T}}([\mathbf{N}^y_{r,j}] - [\mathbf{N}^y_{s,j}])\\
[\mathbf{N}^y_{s,j}] &= [\cdots \quad 0 \quad N_1 \quad 0 \quad 0 \quad N_2 \quad 0 \quad 0 \quad N_3 \quad 0 \quad 0 \quad N_4 \quad 0 \quad 0 \quad N_5 \quad 0 \quad 0 \quad N_6\\
&\qquad 0 \quad 0 \quad N_7 \quad 0 \quad 0 \quad N_8 \quad 0 \quad \cdots]\\
\mathbf{K}_{rs,Z,i,j} &= k_{rs,z}([\mathbf{N}^z_{r,j}] - [\mathbf{N}^z_{s,j}])^{\mathrm{T}}([\mathbf{N}^z_{r,j}] - [\mathbf{N}^z_{s,j}]),\\
[\mathbf{N}^z_{s,j}] &= [\cdots \quad 0 \quad 0 \quad N_1 \quad 0 \quad 0 \quad N_2 \quad 0 \quad 0 \quad N_3 \quad 0 \quad 0 \quad N_4 \quad 0 \quad 0 \quad N_5 \quad 0 \quad 0\\
&\qquad N_6 \quad 0 \quad 0 \quad N_7 \quad 0 \quad 0 \quad N_8 \quad \cdots]
\end{aligned}$$

where s,$t$and $g$denote respectively the longitudinal-, lateral- andvertical- local natural coordinate; the meaning of$n_j$is equal to that explained in Equation (5); the damping matrices$\mathbf{C}_{ss',X,i}$,$\mathbf{C}_{ss',Y,i}$and $\mathbf{C}_{ss',Z,i}$have the same expressions as$\mathbf{K}_{ss',X,i}$,$\mathbf{K}_{ss',Y,i}$and $\mathbf{K}_{ss',Z,i}$just needing to substitute the stiffness coefficients'$k_{ss',x}$','$k_{ss',y}$'and '$k_{ss',z}$'with the damping coefficients'$c_{ss',x}$','$c_{ss',y}$'and '$c_{ss',z}$'.

3.3.2. Interaction matrices between the sleeper and the subgrade

The interaction stiffness and damping matrices, $\mathbf{K}_{ss'}$ and $\mathbf{C}_{ss'}$, between the sleeper and the constraint subgrade can be harvested by

$$\begin{cases} \mathbf{K}_{ss'} = \sum_i \sum_k (\mathbf{K}_{ss',X,i} + \mathbf{K}_{ss',Y,i} + \mathbf{K}_{ss',Z,i}) \\ \mathbf{C}_{ss'} = \sum_i \sum_k (\mathbf{C}_{ss',X,i} + \mathbf{C}_{ss',Y,i} + \mathbf{C}_{ss',Z,i}) \end{cases} \tag{8}$$

with

$$\mathbf{K}_{ss',X,i} = k_{ss',x} \int_{-w_s/2}^{w_s/2} \int_{-l_H/2}^{l_H/2} [\mathbf{N}_{ss'}^x]^{\mathrm{T}} [\mathbf{N}_{ss'}^x] \mathrm{d}z_s \mathrm{d}y_s$$

$$\mathbf{K}_{ss',Y,i} = k_{ss',y} \int_{-w_s/2}^{w_s/2} \int_{-l_H/2}^{l_H/2} [\mathbf{N}_{ss'}^y]^{\mathrm{T}} [\mathbf{N}_{ss'}^y] \mathrm{d}z_s \mathrm{d}y_s$$

$$\mathbf{K}_{ss',Z,i} = k_{ss',z} \int_{-w_s/2}^{w_s/2} \int_{-l_H/2}^{l_H/2} [\mathbf{N}_{ss'}^z]^{\mathrm{T}} [\mathbf{N}_{ss'}^z] \mathrm{d}z_s \mathrm{d}y_s \quad [\mathbf{N}_{ss'}^x] = [\mathbf{N}_{s,j}^x],$$

$$[\mathbf{N}_{ss'}^y] = [\mathbf{N}_{s,j}^y] \text{ and } [\mathbf{N}_{ss'}^z] = [\mathbf{N}_{s,j}^z], \text{ in } [\mathbf{N}_{ss'}^x] \text{ and } [\mathbf{N}_{ss'}^y],$$

$$s = 1, t = y_s/(w_s/2),\ g = z_s/(l_H/2),\ [\mathbf{N}_{ss'}^z],\ s = x_s/(l_W/2) t = y_s/(w_s/2),\ g = 1,$$

where k denotes the number of solid elements for a sleeper; the damping matrices $\mathbf{C}_{ss',X,i}$, $\mathbf{C}_{ss',Y,i}$ and $\mathbf{C}_{ss',Z,i}$ have the same expressions as $\mathbf{K}_{ss',X,i}$, $\mathbf{K}_{ss',Y,i}$ and $\mathbf{K}_{ss',Z,i}$ just needing to substitute the stiffness coefficients '$k_{ss',x}$', '$k_{ss',y}$' and '$k_{ss',z}$' with the damping coefficients '$c_{ss',x}$', '$c_{ss',y}$' and '$c_{ss',z}$'.

4. Methodologies for the model dynamics solution

4.1. Frequency response function (Receptance)

To gain an insight of the characteristics of the coupled system in the frequency domain, the frequency response function will be analysed. After assembling the components of the mass, stiffness and damping matrices to obtain the global system matrices, the governing equations of the vehicle-track system can be written as follows in matrix form:

$$\mathbf{M}\ddot{\mathbf{x}} + \mathbf{K}\mathbf{x} + \mathbf{C}\dot{\mathbf{x}} = \mathbf{f} \tag{9}$$

where $\mathbf{M}$, $\mathbf{K}$, $\mathbf{C}$ are the $N \times N$ global mass, stiffness and damping matrices, respectively. In addition, $\mathbf{x} = [x_1, \cdots, x_m, \cdots, x_n, \cdots, x_N]^T$ is the displacement vector and $\mathbf{f} = [f_1, \cdots, f_m, \cdots, f_n, \cdots, f_N]^T$ is the force vector. If harmonic forces are considered, the force vector can be written as

$$\mathbf{f} = \mathbf{F} \cdot \exp(\mathrm{i}\Omega t) = [F_1, \cdots, F_m, \cdots, F_n, \cdots, F_N]^T \cdot \exp(\mathrm{i}\Omega t) \tag{10}$$

where $\mathbf{F}$ is the amplitude vector of the force and Ω is the frequency of the applied load. Correspondingly, the response can be written as

$$\mathbf{x} = \mathbf{X} \cdot \exp(\mathrm{i}\Omega t) = [X_1, \cdots, X_m, \cdots, X_n, \cdots, X_N]^T \cdot \exp(\mathrm{i}\Omega t) \tag{11}$$

where $\mathbf{X}$ is the amplitude vector of the displacement. Although the proposed three-dimensional model can deal with non-identical excitation on the left and right rails, in this work the receptance due to symmetric point excitations on both rails is calculated, i.e. two unit point loads on the left and right rail heads at the same longitudinal coordinate respectively are considered. Assuming the two unit point loads $f_m = F_m \cdot \exp(\mathrm{i}\Omega t) = 1 \cdot \exp(\mathrm{i}\Omega t)$ and $f_n = F_n \cdot \exp(\mathrm{i}\Omega t) = 1 \cdot \exp(\mathrm{i}\Omega t)$ are applied on the left and right rails at the mth and nth DoFs respectively, upon substitution of the force to Equation (9), one obtains:

$$[-\mathbf{M}\Omega^2 + \mathbf{K} + \mathrm{i}\Omega\mathbf{C}]\mathbf{X} = \mathbf{F} \tag{12}$$

where $\mathbf{F} = [F_1, \cdots, F_m, \cdots, F_n, \cdots, F_N]^T = [0, \cdots, 1, \cdots, 1, \cdots, 0]^T$, the response X_q of an arbitrary qth degree of freedom ($1 \leq q \leq N$) can be obtained by solving Equation (12).

4.2. Time-domain response solution

With consideration of a vehicle moving on the tracks and the nonlinearity of wheel-rail contacts in geometry and force, step-by-step time integral scheme is used to obtain the time-dependent solution of vehicle-track interactions.

Houbolt method is a kind of unconditionally stable implicit integration algorithm, its acceleration and velocity finite difference expansion formula can be expressed as

$$\begin{cases} [\ddot{\mathbf{x}}_{t+\Delta t}] = \dfrac{1}{\Delta t^2}(2[\mathbf{x}_{t+\Delta t}] - 5[\mathbf{x}_t] + 4[\mathbf{x}_{t-\Delta t}] - [\mathbf{x}_{t-2\Delta t}]) \\ [\dot{\mathbf{x}}_{t+\Delta t}] = \dfrac{1}{6\Delta t}(11[\mathbf{x}_{t+\Delta t}] - 18[\mathbf{x}_t] + 9[\mathbf{x}_{t-\Delta t}] - 2[\mathbf{x}_{t-2\Delta t}]) \end{cases} \tag{13}$$

Introduce the above formula into the dynamic equations of motion for vehicle-track interaction, one can get

$$\begin{aligned} &\left(\frac{2}{\Delta t^2}[\mathbf{M}] + \frac{11}{6\Delta t}[\mathbf{C}] + [\mathbf{K}]\right)[\mathbf{x}_{t+\Delta t}] = [\mathbf{R}_{t+\Delta t}] + \left(\tfrac{5}{\Delta t^2}[\mathbf{M}] + \tfrac{3}{\Delta t}[\mathbf{C}]\right)[\mathbf{x}_t] \\ &- \left(\frac{4}{\Delta t^2}[\mathbf{M}] + \frac{3}{2\Delta t}[\mathbf{C}]\right)[\mathbf{x}_{t-\Delta t}] + \left(\tfrac{1}{\Delta t^2}[\mathbf{M}] + \tfrac{1}{3\Delta t}[\mathbf{C}]\right)[\mathbf{x}_{t-2\Delta t}] \end{aligned} \tag{14}$$

From Equation (12), it can be seen that three steps' displacement vector responses, i.e. $[\mathbf{x}_t]$, $[\mathbf{x}_{t-\Delta t}]$, $[\mathbf{x}_{t-2\Delta t}]$ should obtained as preconditions, thus this algorithm will be started by other integration schemes.

5. Numerical studies

In the numerical studies, the vehicle speed to be 200 km/h unless otherwise stated. The time step size used in the time-domain integration is 10^{-4} sec. The vehicle and track parameters are listed in the Appendix; and the system performance of the vehicle and the tracks in time- and frequency- domain will be investigated.

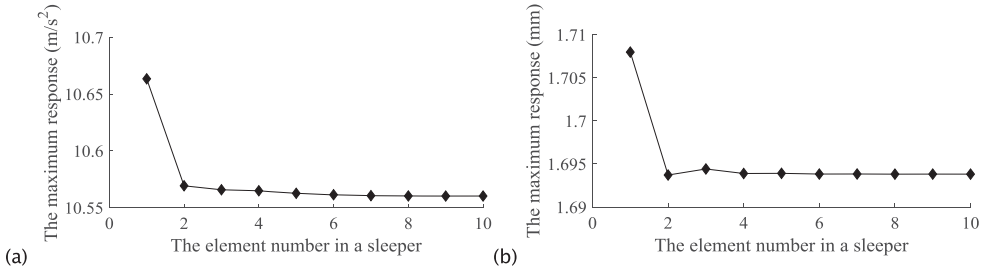

Figure 3. Maximum response of the sleeper against the element number of an elastic-beam sleeper (a. vertical acceleration; b. vertical displacement).

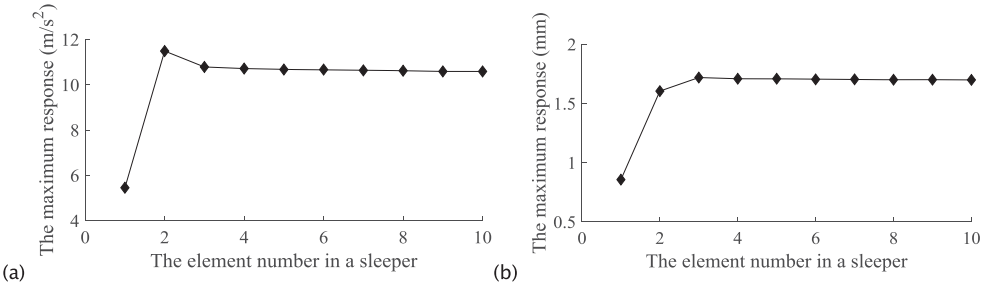

Figure 4. Maximum response of the sleeper against the element number of a solid element sleeper (a. vertical acceleration; b. vertical displacement).

5.1. Confirmation of the number of finite elements in a sleeper

For the sleeper elements established by elastic-beam and solid element, it is of necessity to confirm the minimum element number in constructing the sleeper system with guarantee of both the solution precision and efficiency.

It is known that the dynamic performance of a structure is directly influenced by its own dynamic characteristics. Figures 3 and 4 therefore show the maximum displacement and acceleration responses of a sleeper against different sleeper element numbers. It can be clearly seen from Figures 1 and 2 that when the sleeper element number reaches 4–6, the maximum sleeper vibration responses are basically convergent to a specific value and only with very slight deviations. It is therefore can be concluded that the minimum sleeper element number can be chosen as 4 to promote the computational efficiency in this work.

5.2. Influence of the finite elemental type of the sleeper on system responses

5.2.1. Receptance analysis

In this section the receptances of both the rail and the sleeper are analysed for vertical and lateral motions. Symmetric unit point loadings which are stationary on the left and right rails are considered.

5.2.1.1. Influence on dynamics of the rail. In Figure 5 the receptances of vertical motion of the rail are presented. Symmetric unit point loads are applied vertically on both rails at the

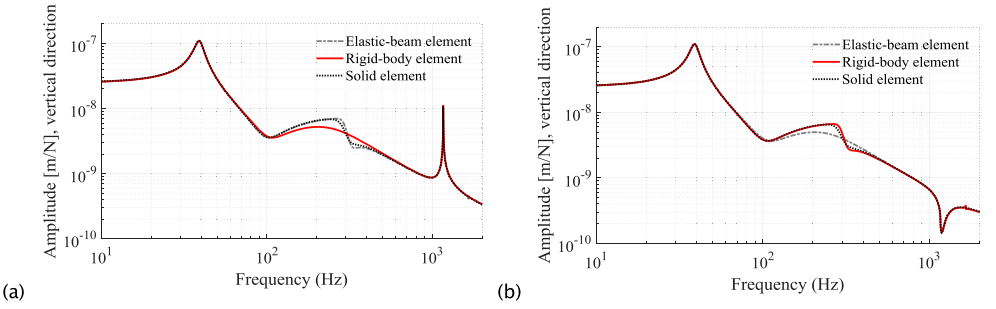

Figure 5. Driving point receptance of the vertical motion of the rail (a. stationary load at mid-span; b. stationary load above a sleeper).

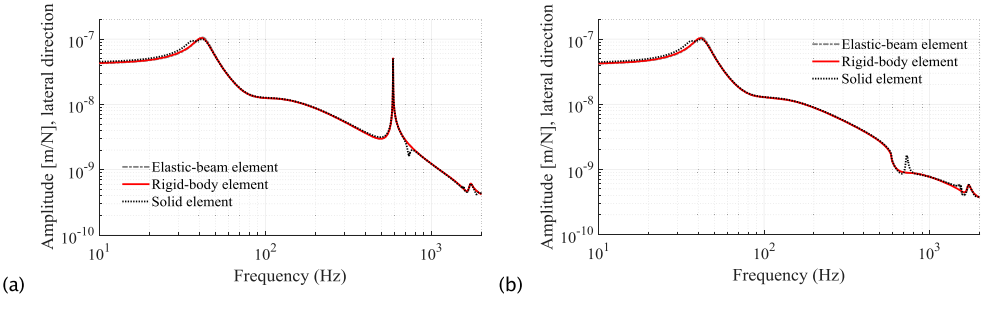

Figure 6. Driving point receptance of the lateral motion of the rail (a. stationary load at mid-span; b. stationary load above a sleeper).

same longitudinal position. Because of symmetry of the applied loads, the receptance on the left rail and right rail are the same. Therefore, one can chose either receptance of the left rail or the right rail. The first peak at around 40 Hz corresponds to the rigid-body motion of the sleeper. The rail and the sleeper vibrates in phase. At about 1080 Hz, pinned-pinned resonance occurs. It can be concluded that the type of sleeper elements have no influences on the rigid-body motion and pinned-pinned mode as expected. On the contrary, in the range of 100–400 Hz, considering the sleeper as rigid gives poor prediction since elastic deformation of sleepers occurs in this frequency range.

Figure 6 shows the influence of element types of sleepers on lateral motion of rails. Symmetric unit point loads are applied laterally on both rails at the same longitudinal position. Similar to that of vertical motion, the two major peaks at 40 and 600 Hz correspond to rigid-body and pinned-pinned motions in the lateral direction, respectively. The predictions resulting from the elastic beam element and rigid-body element are in good agreement till 2000Hz. However, consideration of solid element leads to extra peaks and dips after the pinned-pinned frequency.

5.2.1.2. Influence on dynamics of the sleeper. The receptances of vertical motion of sleepers are shown in Figure 7. In Figure 7 (a), results obtained from rigid-body element and elastic beam element are compared. For the case of elastic beam element, two points are investigated, namely the centre of the sleeper and the point of sleeper under rail fastener. For each peak and dip of the elastic beam case, the deformation pattern of the sleeper is

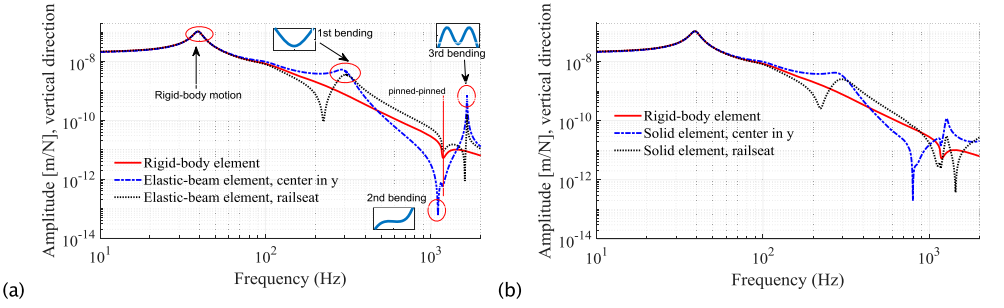

Figure 7. Receptance of the vertical motion of a sleeper, stationary load on the track above the sleeper (a. rigid-body versus beam element; b. rigid-body versus solid element).

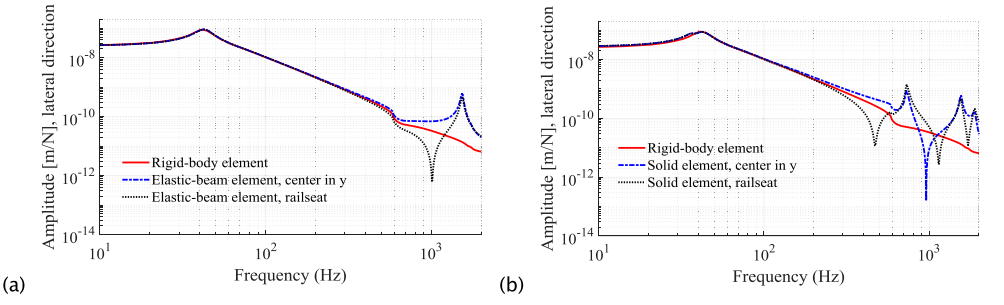

Figure 8. Receptance of the lateral motion of a sleeper, stationary load on the track above the sleeper (a. rigid-body versus beam element; b. rigid-body versus solid element).

plotted. It can be concluded from Figure 7 (a) that it is not adequate to consider the sleeper as rigid since only the predictions of the rigid-body motion and the pinned-pinned motion are accurate. The elastic motions of sleepers which can occur below and above the pinned-pinned frequency should be taken into account. In Figure 7 (b), the predictions by applying solid element for sleepers are compared with those from rigid-body element. Implementing solid element gives similar predictions to those of Euler-Bernoulli beam element. However, generally solid element leads to lower natural frequencies of the sleeper. Moreover, comparing results between Figure 7 (a) and (b), it is shown that Euler-Bernoulli beam element is not an accurate assumption after the pinned-pinned frequency for modelling vibrations of sleepers.

The same comparison is made for the lateral motion of sleepers in Figure 8. Both the rigid-body element and elastic beam element give poor predictions above 300 Hz comparing with results from solid element.

5.2.2. Time-domain response analysis

In the time domain analysis, track irregularities realistically measured from a railway line in China with spatial sampling interval of 0.25 m are loaded as the system excitation, as shown in Figure 9.

In Figures 10 and 11, the time-varying wheel-rail vertical and lateral forces with regarding to various sleeper finite elements are presented. It can be seen from these two figures that the wheel-rail vertical forces derived by the elastic-beam element model and the solid

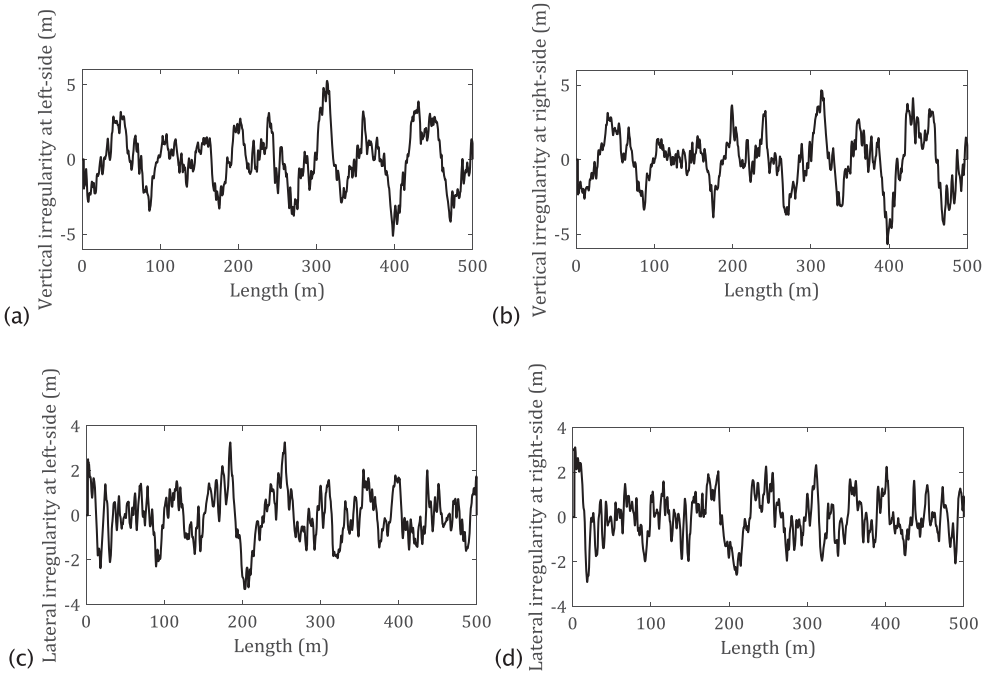

Figure 9. Track irregularity excitation (a. vertical irregularities at the left-side of the rail; b. vertical irregularities at the right-side of the rail; c. lateral irregularities at the left-side of the rail; d. lateral irregularities at the right-side of the rail).

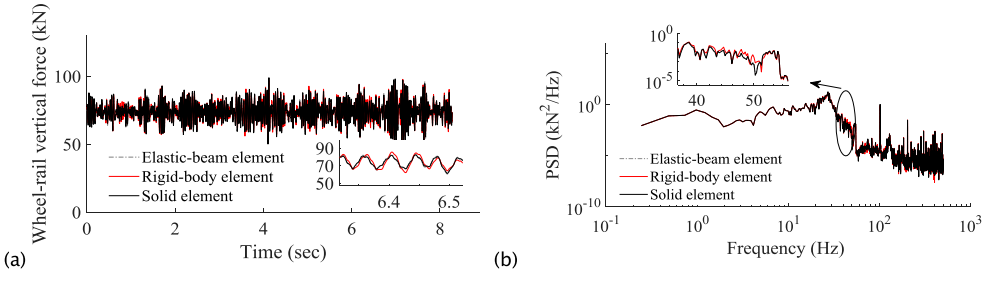

Figure 10. Comparison on wheel-rail vertical forces (a. time-domain responses; b. PSD).

element model approach to each other with a higher degree comparing to that of the rigid-body element model, in general, the maximum response of the rigid-body element model is relatively larger than those of the other two models but within a maximum difference of 5 kN. Being different to the wheel-rail vertical forces, the wheel-rail lateral forces of the elastic-beam element model and the rigid-body element model coincide well with each other comparing to those derived by the solid element model, but the difference is also actually very small, the maximum responses difference is smaller than 2 kN.

From the Figures 10 and 11, it can be cognised that it causes difference of the wheel-rail forces due to the choices of difference sleeper finite element types, but the difference is

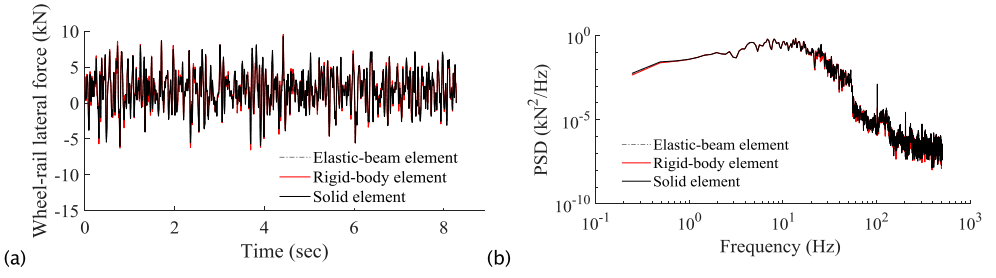

Figure 11. Comparison on wheel-rail lateral forces (a. time-domain responses; b. PSD).

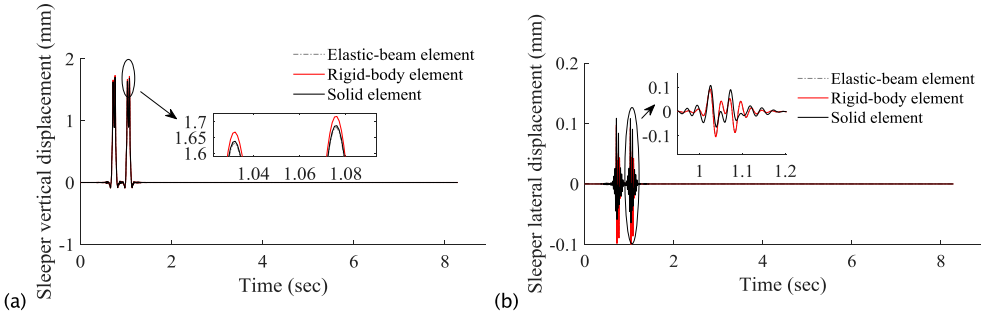

Figure 12. Sleeper displacement against different sleeper finite elements (a. sleeper vertical displacement; b. sleeper lateral displacement).

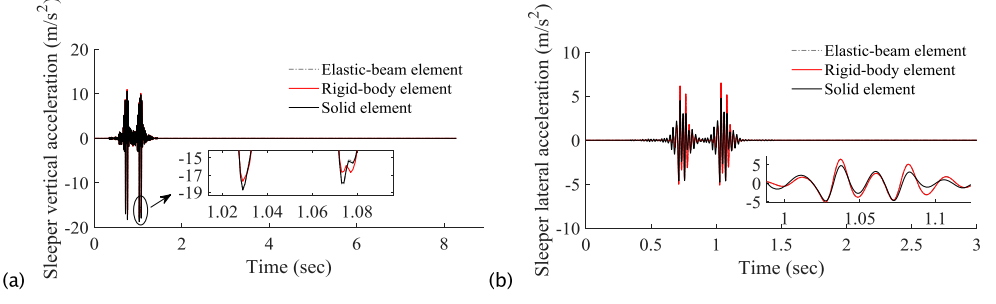

Figure 13. Sleeper acceleration against different sleeper finite elements (a. sleeper vertical acceleration; b. sleeper lateral acceleration).

generally in a small variation range. Obvious the influence of sleeper finite element types shows slight effects on vehicle dynamics behaviours.

The sleeper fix-point vibrations are shown in Figures 12 and 13. It can be observed from Figure 12 that the sleeper displacements of different finite element types possess different vibration characteristics, where the maximum vertical displacement for the elastic-beam, rigid-body and solid element sleeper are respectively 1.721, 1.70 and 1.73 mm, and the maximum lateral displacement for the elastic-beam, rigid-body and solid element sleeper are respectively 0.105, 0.093 and 0.108 mm. Obviously the vibrational displacement of the elastic-beam and solid element sleeper coincide well with each other in response amplitudes.

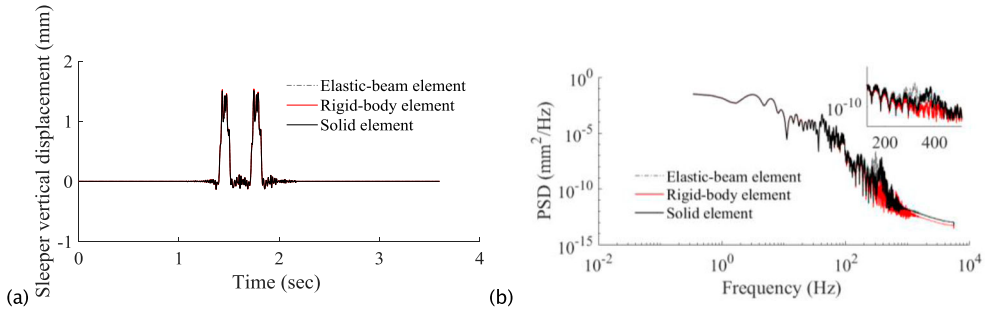

Figure 14. Comparison on sleeper vertical displacement at centroid (a. time-domain responses; b. PSD).

Figure 13 illustrates the sleeper vertical and lateral acceleration respectively. It can be observed from Figure 13 (a) that the vertical acceleration of the elastic-beam and the solid element approaches to each other with absolute maximum value of 18.71 and 18.73 m/s^2, while the vertical acceleration of the rigid-body sleeper is a little smaller with absolute maximum value of 17.25 m/s^2. As to the sleeper lateral acceleration, the absolute maximum values for the elastic-beam, rigid-body and solid elemental sleeper are respectively 6.526, 4.735 and 6.452 m/s^2 respectively, namely the lateral vibrations of the sleeper derived by the elastic-beam and the solid element are much closer comparing to that derived by the rigid-body sleeper.

Moreover, the short wavelength irregularities can be also considered to illustrate the influence of sleeper elements on system responses at high frequencies, where the short wavelength track irregularities are simulated by spectral density function below [22]

$$S(f) = Af^B \tag{15}$$

where A and B are short wavelength irregularity spectrum parameters; f is the spatial frequency with unit: m^{-1}. The minimum sampling interval of short wavelength track irregularities is 0.005 m, and its effective wavelength range is from 0.01 m to 0.50 m.

In the high frequency analysis, an emphasis is put on clarifying the sleeper finite elements on sleeper vibrations. Figures 14 and 15 show the vertical and lateral displacements of a sleeper at the centroid, respectively. It can be clearly seen from Figures 14 and 15 that the sleeper displacements regarding various sleeper finite elements show slight difference at low frequency domain, but it can be observed that a large difference becomes obvious at frequency higher than 230 Hz. As to the sleeper vertical displacement, the results derived by the rigid body element are smaller than those derived by elastic-beam and solid element at high frequency domain, while for the sleeper lateral displacement, the results derived by the rigid body element are larger than those derived by other two elements. Moreover it can be seen that the difference between the sleeper lateral displacements of the rigid body element and the solid element is relatively small, while to the sleeper vertical displacement, it can be noticed that the peak frequency of power spectral density (PSD) for the sleeper beam element and solid element is respectively 305 and 370 Hz, that is, there still exists difference between the elastic beam element and the solid element.

Figures 16 and 17 further illustrate the result comparison on sleeper accelerations, from which it can be seen that the peak frequencies of PSD of the elastic beam element and the

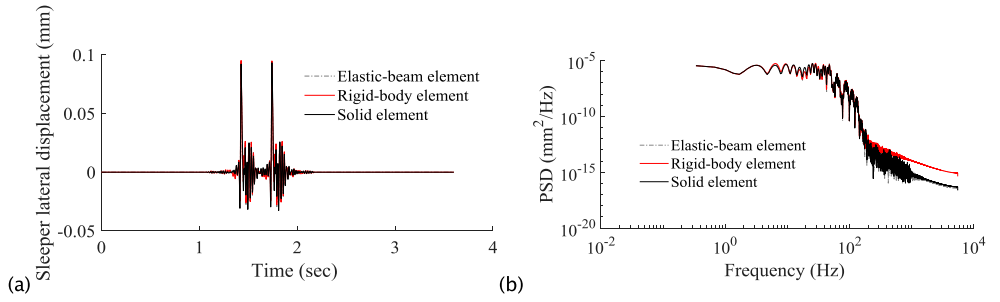

Figure 15. Comparison on sleeper lateral displacement at centroid (a. time-domain responses; b. PSD).

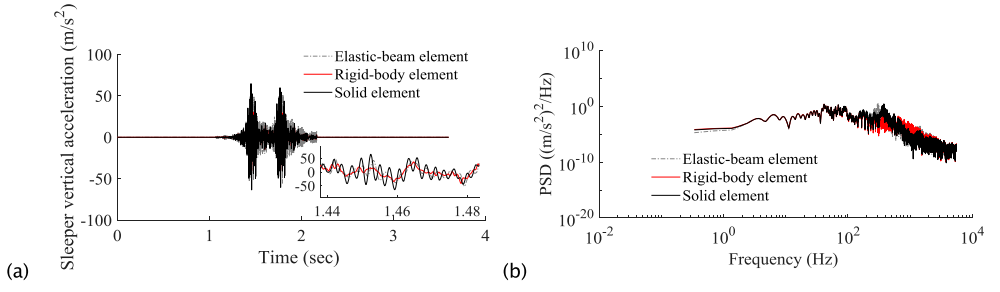

Figure 16. Comparison on sleeper vertical acceleration (a. time-domain responses; b. PSD).

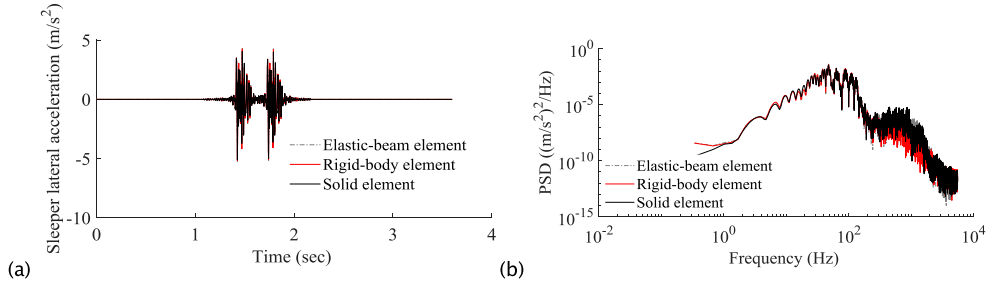

Figure 17. Comparison on sleeper lateral acceleration (a. time-domain responses; b. PSD).

solid element are respectively 304 and 371 Hz, which are close to those of the sleeper displacement PSD distribution as elaborated above. Besides, it can be seen from Figure 16 (a) that the sleeper vertical acceleration of solid elements fluctuates more violently than those by rigid body elements and elastic-beam element. As to sleeper lateral acceleration, the rigid body acceleration is generally lower than those using elastic beam and solid elements at high frequency domain.

5.2.3. Influence of the support stiffness and damping coefficients of the ballast

Set the support stiffness coefficient of the track bed to be varied from 10 MN/m to 100 MN/m with an interval of 10 MN/m with constant support damping coefficient of track bed. Figure 18 shows the maximum system response for different dynamic indices such

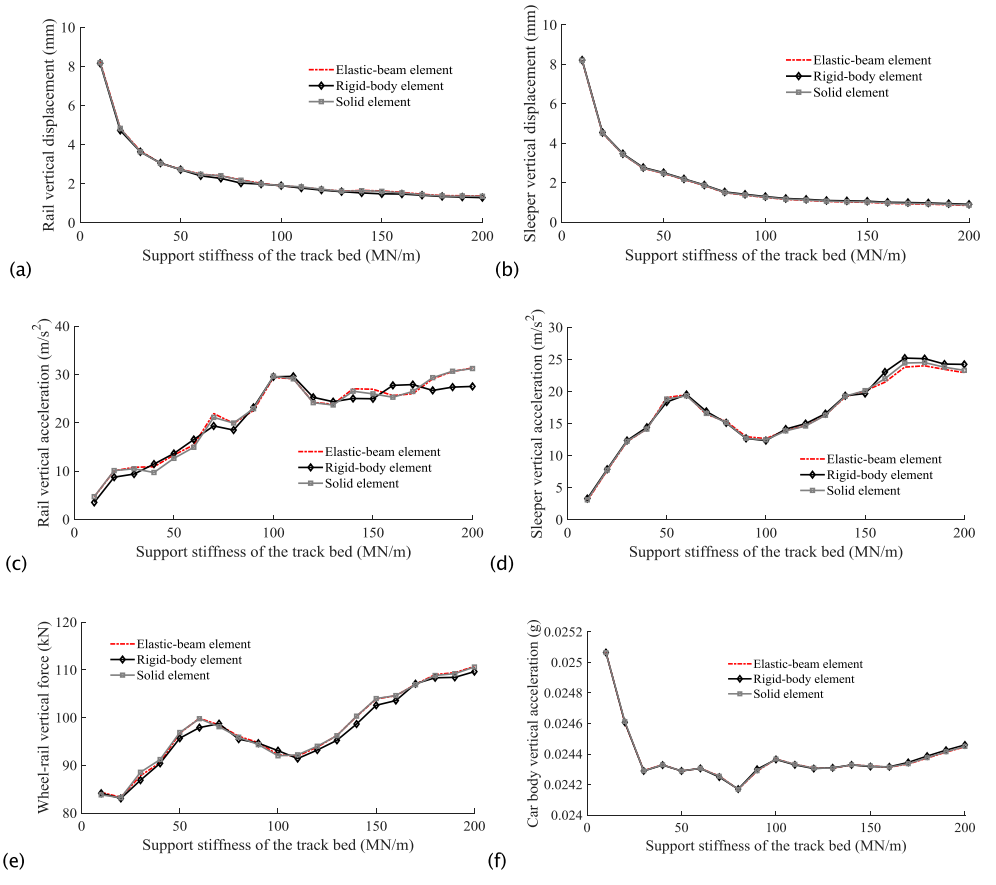

Figure 18. The maximum responses of system indices against the increasing of vertical support stiffness coefficients of the track bed (a. rail vertical displacement; b. sleeper vertical displacement; c. rail vertical acceleration; d. sleeper vertical acceleration; e. wheel-rail vertical force; f. car body vertical acceleration).

as the rail and the sleeper acceleration and displacement, the wheel-rail force and the car body acceleration.

The results shown in Figure 18 (a) and (b) indicate that all sleeper finite elements have almost the same changing treads against the increasing the track bed support stiffness, where the rail and the sleeper displacements are gradually decreased, and the displacement responses with respect to various sleeper finite element types are actually rather small. Being contrary to the changing rule of rail and sleeper displacement, the rail and sleeper accelerations are generally increased by the enlargement of the track bed support stiffness, as shown in Figure 18 (c) and (d). Besides it can be noticed that the acceleration deviation is more obvious comparing to those of the displacement response between different sleeper finite element types, also, the maximum accelerations derived by models with the sleeper elastic-beam element and solid element are significantly approaching to each other comparing to those derived by the model with the rigid-body element of sleepers. When the support stiffness of the track bed reaches the maximum value of 200 MN/m, the rail maximum vertical accelerations for the elastic-beam, rigid-body and solid sleeper element

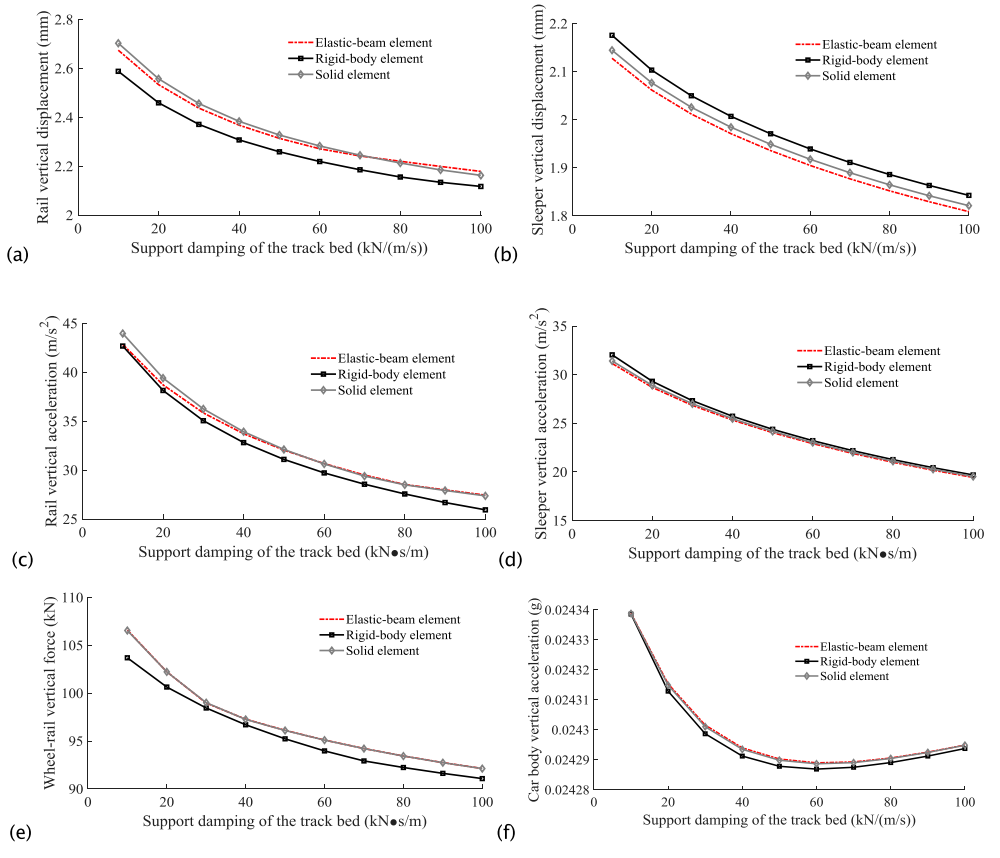

Figure 19. The maximum responses of system indices against the increasing of vertical support damping coefficients of the track bed (a. rail vertical displacement; b. sleeper vertical displacement; c. rail vertical acceleration; d. sleeper vertical acceleration; e. wheel-rail vertical force; f. car body vertical acceleration).

are respectively 32.1, 27.6 and 32.0 m/s^2, and it seems that the sleeper acceleration deviations between different sleeper finite element models are more and more noticeable when the track bed support stiffness coefficient is larger than 150 MN/m.

Apart from the track vibrations, Figure 18 (e) and (f) respectively illustrate maximum response treads of wheel-rail vertical force and car body vertical acceleration. It can be seen that the track bed support stiffness exposes significantly influence on wheel-rail vertical forces. When the track bed support stiffness is increased from 10 MN/m to 200 MN/m, the maximum wheel-rail vertical is increased by about 37.56%. Similarly the response amplitudes corresponding to the elastic-beam element and the solid element are rather approachable to each other comparing to that of the rigid-body element. The car body acceleration is also influence by the track bed support stiffness but in a rather small extent.

Setting the support damping coefficient of the track bed to be varied from 10 kN/(m/s) to 100 kN/(m/s) with an interval of 10 kN/(m/s), Figure 19 shows the system maximum responses also for indices of rail and sleeper vertical displacement and acceleration, wheel-rail vertical force and car body vertical acceleration. With the increasing of the damping

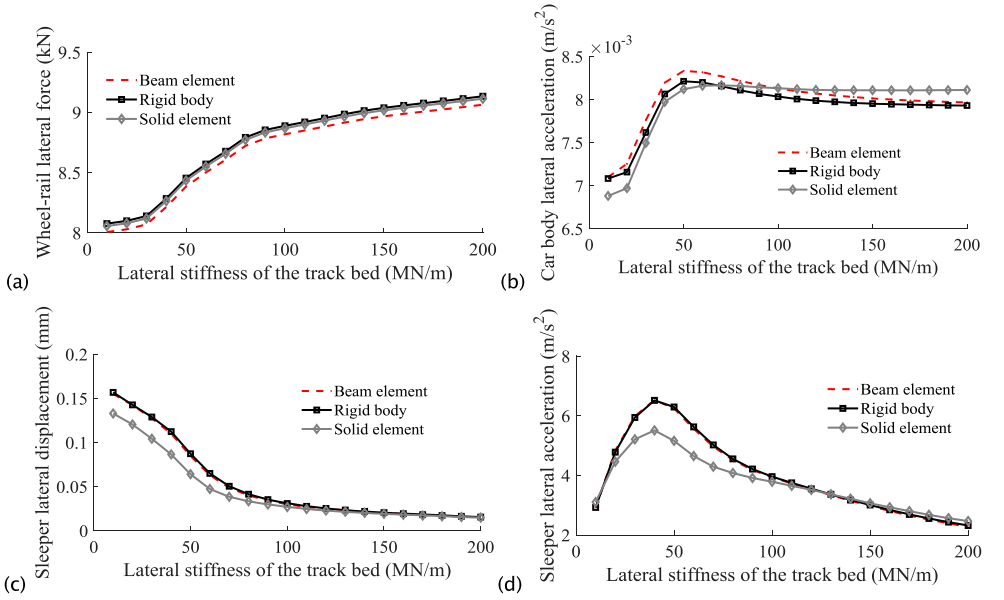

Figure 20. The maximum responses of system indices against the increasing of lateral stiffness coefficients of the track bed (a. wheel-rail lateral force; b. car body lateral acceleration; c. sleeper lateral displacement; d. sleeper lateral acceleration).

coefficient of the track bed, the response amplitudes of the presented indices are all generally decreased. Moreover, to different dynamic indices, the influence degree of the sleeper finite elements is also a little different. For example, the rail vertical vibrations corresponding to the model with sleeper rigid-body element, as shown in Figure 19 (a) and (b) is obviously smaller than those with sleeper elastic-beam and solid elements, and the maximum difference is about 0.13 mm and 2.2 m/s^2, besides, with the increasing of the support damping of the track bed, the response amplitudes derived by the models with the elastic-beam element and the solid element gradually approach to each other. With almost the same law, the wheel-rail forces of the elastic-beam and solid element models are almost the same but relatively larger than that of the rigid-body element model.

The influence of lateral stiffness and damping coefficients of the track bed on the system dynamic performance can be also assessed. As an example, Figure 20 shows the maximum responses of wheel-rail force, car body acceleration and sleeper displacement and acceleration at the lateral direction against the increase of the lateral resistance stiffness of the track bed. It can be seen from Figure 20 (a) that the wheel-rail lateral force is increased by increasing the lateral stiffness coefficient of the track bed for all sleeper element types. While to the sleeper lateral displacement, as shown in Figure 20 (c), it is gradually decreased by the increase of the lateral stiffness of the track bed, besides, it can be seen that the maximum responses of the sleeper lateral displacement derived by the solid sleeper are smaller than those derived by the other two sleeper types especially for small lateral stiffness coefficients. Moreover it is interesting to see that the car body lateral acceleration and the sleeper lateral acceleration both experience a process of first rise and then falling, and the responses reach the maximum values when the lateral stiffness reaches 40–50 MN/m.

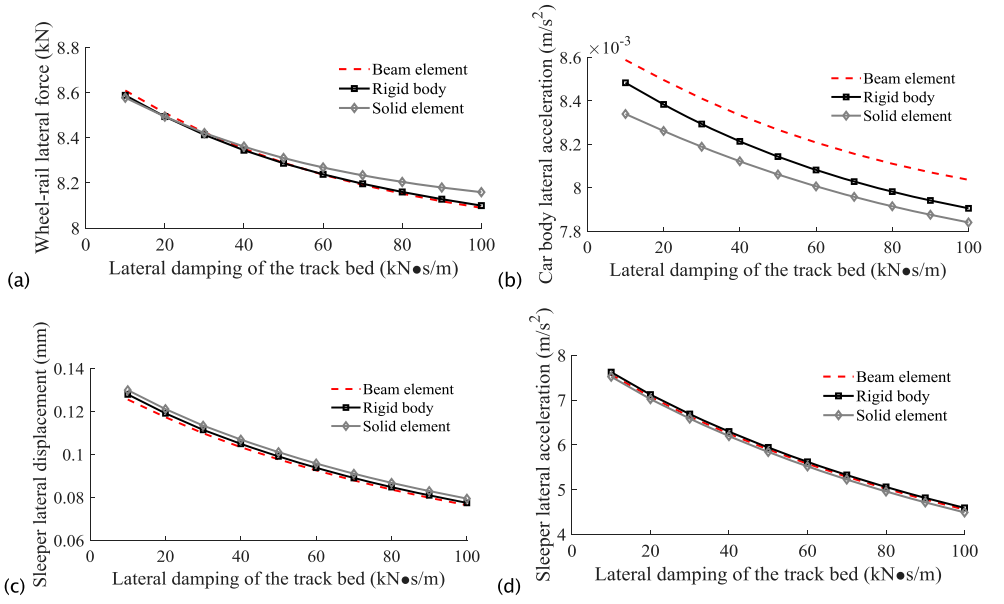

Figure 21. The maximum responses of system indices against the increasing of lateral damping coefficients of the track bed (a. wheel-rail lateral force; b. car body lateral acceleration; c. sleeper lateral displacement; d. sleeper lateral acceleration).

Moreover, Figure 21 shows the maximum responses of wheel-rail force, car body acceleration and sleeper displacement and acceleration at the lateral direction for different lateral damping coefficient of the track bed. From the figure it can be seen that the maximum responses of all dynamic indices are attenuated gradually accompanied by the increasing of the lateral damping of the track bed. As to different finite element types, it can be observed that the sleeper finite element type also shows inevitable effects on system lateral vibrations but the difference is generally smaller than 10%.

6. Conclusion

In this work, the influence of the sleeper finite element types on system dynamic behaviours is investigated in detail based on numerical studies on the time- and frequency-domain. Apart from model validations, several conclusions can be drawn as follows:

(1) The elastic deformation is of significance for vibrations of both rails and sleepers. The influence of element types of modelling sleepers on dynamics of sleepers is greater than that on rails. The 1st bending motion of sleepers in vertical direction falls in between the in-phase rigid-body resonance and the pinned-pinned frequencies. The elastic motion of sleepers in lateral direction plays an important role after 300 Hz. Summarily elastic motions of sleepers need to be taken into account in the middle and high frequencies ranges for both vertical and lateral motions.
(2) The sleeper elemental types representing different elasticity and vibration characteristics. Generally the sleeper model built by elastic beams can obtain approachable results to those derived by solid element model but with higher computational efficiency, and

the track vibrations with rigid-body sleepers show relatively large differences to elastic sleepers.

(3) The sleeper element type shows little influence on wheel-rail interaction and vehicle vibrations but mainly affecting the track structural performance. However the support stiffness and damping coefficients of track bed both in vertical and lateral directions show non-negligible effects on the whole system's dynamic behaviours. For larger vertical support stiffness, the smaller of the rail and sleeper displacement, but the larger of the acceleration, and the increasing of lateral stiffness will result in lower sleeper lateral displacement and higher wheel-rail lateral force. However, the influence of lateral stiffness of track bed on car-body and sleeper lateral accelerations is not monotonous and there exists a value of stiffness (between 40–50 MN/m) at which the accelerations have a peak. Besides, the increasing of the support damping coefficients in both vertical and lateral directions can significantly reduce the track vibrations in the corresponding direction.

(4) It is noted that in frequency domain the results using rigid body sleeper shows significant differences to those using elastic sleeper elements in the middle to high frequency ranges. However, the differences of the time domain responses using models with different sleeper elements are generally not that large from engineering evaluation viewpoint if the equivalent effective frequency of typical track irregularity excitations has not reached those high frequencies. In line with the frequency-domain response, the time-domain responses using different finite element types are generally different at high frequencies when short wavelength irregularities are considered. Rigid-body modelling for sleepers is not recommended for the case of high frequency excitations.

Disclosure statement

No potential conflict of interest was reported by the author(s).

Funding

This work was supported by the National Natural Science Foundation of China (No.: 51820105014; 51708558; 51578549; 51678576); the National Key R&D Program of China (No. 2017YFB1201204)

ORCID

Tao Lu http://orcid.org/0000-0002-1340-5758

References

[1] Abadi T. Effect of sleeper and ballast interventions on rail track performance. University of Southamption; 2015.

[2] Le Pen L, Zervos A, Powrie W. Effects of sleeper interventions on railway track performance. J Geotech Geoenviron Eng. 2019;145(4):04019009.

[3] Lam HF, Wong MT. Railway ballast diagnose through impact hammer test. Procedia Eng. 2011;14:185–194.

[4] Giannakos K. Damage of railway sleepers under dynamic loads: a case history from the Greek railway network, Sixth International Conference on Case Histories in Geotechnical Engineering, 2008.

[5] Liu R, Emanuele Z, Andrea C. Vision-based measurement of crack generation and evolution during static testing of concrete sleepers. Eng Fract Mech. 2020;224:106715.

[6] Kishore Kuumar D, Sambasivarao K. Static and dynamic analysis of railway track sleeper. Int J Eng Res Gen Sci. 2014;2(6):662–671.
[7] You R, Kaewunruen S. Evaluation of remaining fatigue life of concrete sleeper based on field loading conditions. Eng Fail Anal. 2019;105:70–86.
[8] Sadeghi J. Field investigation on dynamics of railway track pre-stressed concrete sleepers. Adv Struct Eng. 2010;13(1):139–151.
[9] Anderson JS, Rose JG. In-situ test measurement techniques within railway track structures, Proc., IEEE/ASME/ASCE 2008 Joint Rail Conf., ASME, New York, 2008, 187–207.
[10] Song WM, Shu X, Huang BS, et al. Pressure distribution under steel and timber crossties in railway tracks, J Transp Eng Part A: Syst. 2017;143(9):04017046.
[11] Koike Y, Nakamura T, Hayano K, et al. Numerical method for evaluating the lateral resistance of sleepers in ballasted tracks. Soils Found. 2014;54(3):502–514.
[12] Grassie SL. Dynamic modelling of concrete railway sleepers. J Sound Vib. 1995;187(5):799–813.
[13] Tran L-H, Hoang H, Duhamel D, et al. A fast analytical method to calculate the dynamic response of railway sleepers. J Vib Acoust. 2019;141:011005.
[14] Kaewunruen S, Remennikov AM. Nonlinear finite element modelling of railway prestressed concrete sleeper. The Tenth East Asia-Pac Conference Str Eng Constr. 2006;4:323–328.
[15] Sadri M, Lu T, Steenbergen M. Railway track degradation: The contribution of a spatially variant support stiffness-local variation. J Sound Vib. 2019;455:203–220.
[16] Kumaran G, Menon D, Nair KK. Dynamic studies of railtrack sleepers in a track structure system. J Sound Vib. 2003;268(3):485–501.
[17] Zhai W, Wang K, Cai C. Fundamentals of vehicle-track coupled dynamics. Veh Syst Dyn. 2009;47(11):1349–1376.
[18] Xu L, Chen X, Li X, et al. Development of a railway wagon-track interaction model: case studies on excited tracks. Mech Syst Signal Process. 2018;100:877–898.
[19] Xu L, Yu Z, Shi C. A matrix coupled model for vehicle-slab track-subgrade interactions at 3-D space. Soil Dyn Earthq Eng. 2020;128:105894.
[20] Nielsen JCO, Oscarsson J. Simulation of dynamic train-track interaction with state-dependent track properties. J Sound Vib. 2004;275(3–5):515–532.
[21] Shi C, Zhao CF, Zhang X, et al. Coupled discrete-continuum approach for railway ballast track and subgrade macro-meso analysis. Int J Pavement Eng. 2020.
[22] Zhai W. Vehicle-track coupled dynamics theory and Applications. Singapore: Springer; 2020.

Appendix

Table A1. Vehicle parameters.

Item	Value	Units
Wheelset mass [m_w]	2400	kg
Bogie mass [m_b]	3300	kg
Car-body mass [m_c]	48000	kg
Primary stiffness per axle box [k_{px}, k_{py}, k_{pz}]	14.68, 6.47, 1.176	MN/m
Secondary stiffness per axle box [k_{sx}, k_{sy}, k_{sz}]	0.167, 0.167, 0.323	MN/m
Primary damper per axle box [c_{px}, c_{py}, c_{pz}]	0.0, 0.0, 9.8	kN·s/m
Secondary damper per axle box [c_{sx}, c_{sy}, c_{sz}]	67.1, 39.20, 9.8	kN·s/m
Moment of inertia of car-body [I_{cx}, I_{cy}, I_{cz}]	149.97, 2267.76, 2139.90	Mg·m^2
Moment of inertia of bogie [I_{bx}, I_{by}, I_{bz}]	2.67, 1.81, 3.30	Mg·m^2
Moment of inertia of wheelset [I_{wx}, I_{wy}, I_{wz}]	949, 118, 967	kg·m^2
Wheel normal radius [R_w]	0.43	m
Half of wheelbase [l_t]	1.25	m
Half of bogie centroid distance [l_c]	8.75	m

Table A2. The parameters for the ballasted track.

Notation	Parameter	Value	Units
E_r	Elastic modulus of the rail	2.1×10^{11}	Pa
κ	Timoshenko shear coefficient of the rail	0.4	
m_r	Rail mass per unit length	60.64	kg/m
A_r	Rail cross-sectional area	7.67×10^{-5}	m^2
μ	Rail Poisson's ratio	0.3	
L	Sleeper distance	0.6	m
I_0	Torsional inertia of the rail	3.741×10^{-5}	m^4
I_y	Rail second moment of area about the Y axis	3.217×10^{-5}	m^4
I_z	Rail second moment of area about the Z axis	5.24×10^{-6}	m^4
K_r	Rail torsional stiffness	1.9587×10^{5}	N·m/rad
M_s	Sleeper mass (half)	125	kg
$k_{rs,z}$	Fastener stiffness in the vertical direction	1.2×10^{8}	N/m
$k_{rs,y}$	Fastener stiffness in the lateral direction	2.94×10^{7}	N/m
$c_{rs,z}$	Fastener damping in the vertical direction	5.0×10^{4}	N·s/m
$c_{rs,y}$	Fastener damping in the lateral direction	5.2×10^{4}	N·s/m
k_{sy}	Lateral stiffness of the ballast	5.0×10^{7}	N/m
c_{sy}	Lateral damping of the ballast	2.0×10^{4}	N·s/m
k_{sz}	Vertical stiffness of the ballast	5.29×10^{7}	N/m
c_{sz}	Vertical damping of the ballast	2.0×10^{4}	N·s/m
l_s	Sleeper spacing	0.545	m
l_s	Effective support length of the sleeper	1.90	m
w_s	Sleeper width	0.273	m
ρ_b	Ballast density	1.8×10^{3}	kg/m^3
E_b	Elastic modulus of the ballast	1.1×10^{8}	Pa
c_b	Ballast damping	5.88×10^{4}	N·s/m
k_w	Ballast shear stiffness	7.84×10^{7}	N/m
c_w	Ballast shear damping	8.0×10^{4}	N·s/m
α	Ballast stress distribution angle	35	°
h_b	Ballast thickness	0.55	m
E_s	Young's modulus of sleeper for beam element	2.0×10^{10}	Pa
I_{sx}	Sleeper second moment of area about the X axis for beam element	8.942×10^{-4}	m^4
I_{sz}	Sleeper second moment of area about the Z axis for beam element	3.6501×10^{-4}	m^4
A_s	Sleeper cross-sectional area for beam element	0.0828	m^2